



Performance of a Low Speed Axial Compressor Rotor Blade Row under Different Inlet Distortions

Reza Taghavi Zenouz, Mehran Eshaghi Sir, and Mohammad Hosein Ababaf Behbahani

School of Mechanical Engineering, Iran University of Science and Technology,
Narmak, Tehran 16846-13114, Iran

Correspondence to: Reza Taghavi Zenouz (taghavi@iust.ac.ir)

Received: 17 March 2016 – Revised: 23 March 2017 – Accepted: 29 April 2017 – Published: 31 May 2017

Abstract. Responses of an axial compressor isolated rotor blade row to various inlet distortions have been investigated utilizing computational fluid dynamic technique. Distortions have been imposed by five screens of different geometries, but with the same blockage ratio. These screens were embedded upstream of the rotor blade row. Flow fields are simulated in detail for compressor design point and near stall conditions. Performance curves for distorted cases are extracted and compared to the undisturbed case. Flow simulations and consequent performance characteristics show that the worst cases belong to non-symmetric blockages, i.e., those of partial circumferential configurations. These cases produce the largest wakes which can disturb the flow, considerably. Superior performances correspond to the inner and outer continuous circumferential distortion screens. Since, they produce no significant disturbances to the main flow in comparison to the non-symmetric screens.

1 Introduction

Demands on designing gas turbines with high efficiency and stable operation range under various conditions are extensively increasing. Aerodynamic and thermodynamic performances of gas turbines of power stations, aircraft and road vehicles are highly dependent on entrance air flow conditions. The first modulus of a gas turbine is its compressor or fan. There is always an entrance duct, in which, air flow is being directed towards the compressor or fan blades. Dependent on the engine type and its assignment, there might be miscellaneous components and connections which may affect inflow uniformity. In addition, aircraft may be encountered to non-uniformity of the entrance air flow during their manoeuvres. Atmospheric cross wind and ingestion of some foreign objects may also cause the air to enter the engine non-uniformly. In extreme cases, entrance flow distortion and blockage may lead to occurrence of flow instabilities in terms of the stall or surge in their any possible various types. Rotating stall and surge can occur in their different types. Rotating stall can appear either in “spike” or “modal” states and the surge phenomenon is commonly categorized as “mild”, “modified”, “classic” and “deep” types. All these flow instabilities depend on the compressor characteristics and the flow

conditions in the upstream and downstream of the compressor.

All the above-mentioned inlet distortion types cause blockage to the main airstream. Since, the flow may separate from the solid surfaces and as a result, cause the effective area of the flow to decrease. This event can be led to poor operation of the compressor unit and consequent performance deterioration of the gas turbine.

Nowadays, modern engines are designed on the basis of dividing compressor unit to stages with loadings as high as possible. Accordingly, any disturbance upstream the compressor may downgrade its performance, considerably. Therefore, acquiring knowledge on entrance disturbance effects on the compressor or fan performances can be useful for designers during their design process.

There can be found many research works in literature which are devoted to deep insight into the flow mechanism of compressor or fan under distorted conditions. In parallel to experimental investigations, computational fluid dynamics methods have been widely used by researchers. Of effective techniques for simulation of the entrance flow blockage are employing screens of special geometries which can be mounted upstream the compressor. This technique causes

cross sectional non-uniformity in the entrance total pressure, i.e., the same effect as that which may happen in the reality.

Of researchers who have investigated on the effects of inlet flow distortions on axial flow compressor performance can be referred to Charalambous et al. (2004). They showed that key signature of inlet distortion is drop in axial velocity magnitude within the distorted region. This velocity drop can be led to change in some overall parameters such as mass flow rate, pressure ratio and efficiency. In addition, they observed that decrease in axial velocity is accompanied by alternation in local flow direction relative to the rotating blades. As a result, the blade loading may be increased and ultimately the operating point may be shifted towards the surge line. Effects of block type inlet distortion on general performance of a gas turbine engine are studied by Lee et al. (2007, 2010). They observed considerable deterioration of overall performance and stability of the engine together with increased SFC and reduction in the engine thrust force.

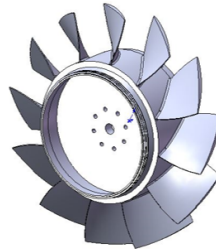
Boundary layer ingestion (BLI) is one of the most important factors in enforcing disturbances to the entry flow of the compression systems of gas turbine engines. BLI literally means ingesting the boundary layer formed on the fuselage and/or wing of aircraft into the intake duct of a propulsion system. Effect of BLI-type inlet distortion on modified JT15D-1 turbofan engine performance has been investigated by Lucas et al. (2014). His results showed 15.5 % decrease in corrected stream thrust and 14 % increase in corrected TSFC in the presence of embedded BLI-type distortion.

Berrier and Allan (2004) have conducted experimental investigations on a S-shape inlet duct with high level of boundary layer ingestion under realistic operating conditions (high subsonic Mach numbers and full-scale Reynolds numbers). They found out that increasing the free-stream Mach number can magnify the disturbances due to the BLI and finally cause the compressor losses to increase.

Inlet distortion under crosswind effects has been numerically investigated by Liu et al. (2014) for a high bypass ratio turbofan engine. They concluded that upstream flow separations, reattachments and induced ground vortices are main sources for the crosswind distortions. Static inflow distortion effects on an axial flow fan performance has been numerically studied by Raj and Pandian (2014). They had focused on development of stall cells and consequent losses within the blades passages. They recorded a reduction of 13.7 % in the total pressure rise due to the inflow distortion.

Generally speaking, inlet distortion can also be happen in terms of non-uniformity in the inlet temperature. Of researchers who have been focused on this subject can be referred to Zhipeng et al. (2015). In parallel to effects of inlet pressure distortion on performance of a new designed fan, they considered effects of inlet temperature distortions through their numerical simulations, too.

Inlet distortion studies are also carried out on high speed compressors. For example, effects of total pressure inlet distortion on the flow field of a transonic compressor rotor blade



Parameter	Value
Rotational speed (rpm)	1300
Hub diameter (mm)	270
Hub to tip ratio	0.6
Tip clearance/blade chord (%)	1.7
Tip chord length (mm)	117.5
Blade tip solidity	1
Tip stagger angle (deg)	56.2

Figure 1. Rotor blade row geometry and specifications.

row, was investigated experimentally and numerically (Hah et al., 1998). They found that there are very strong interactions between the unsteady passage shock and the blade boundary layer. These interactions amplify passage blockage, and as a result, cause aerodynamic losses to be increased and stall margin to be reduced.

Implementation of control methods in order to decrease instabilities produced due to the inlet distortion is investigated in limited studies. Among stability control methods, casing treatment as a passive control method in its various forms is a popular technique which is used extensively in axial compressors. For example, Dong et al. (2015) through their experimental research work on rotating inlet distortion effects on a low-speed axial compressor, have improved its performance via stall precursor-suppressed (SPS) casing treatment. Inlet distortion effects on performance of an axial compressor rotor blade row in the presence of casing treatment of circumferential groove type are investigated by Jian and Hu (2008). They concluded that this kind of treatment can expand the compressor rotor operating range either with or without inlet circumferential pressure distortion at the expense of a slight drop in the isentropic efficiency.

In the present research work, three dimensional numerical simulation of flow field in an axial compressor rotor blade row is executed for different distorted inlet flows from far to near stall conditions. Distortions are imposed to the entrance flow by mounting different arrangements of screens upstream the rotor blade row. Performance map and contours of flow properties are extracted from excessive CFD analyses for each inlet distortion case and also for the non-distorted case for comparison.

2 Model and numerical scheme

An isolated rotor blade row of an axial compressor consisted of 12 blades of NACA-65 cross sectional profile is considered for the present numerical task. Figure 1 shows schematic drawing of this blade row together with its general specifications. This rotor blade row has already been tested experimentally by Inoue and Kuroumaru (1989). General performance characteristics of the present rotor blade row are the same as those introduced by Inoue et al.

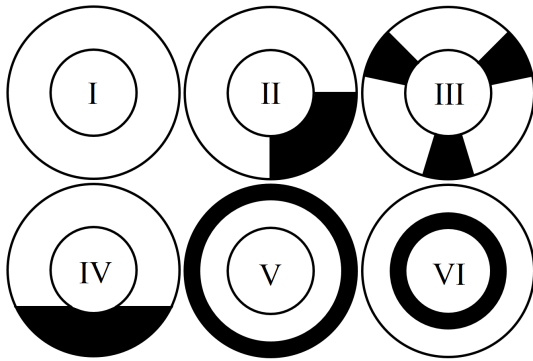


Figure 2. Undistorted inlet (case I) and distortion screens (cases II–VI).

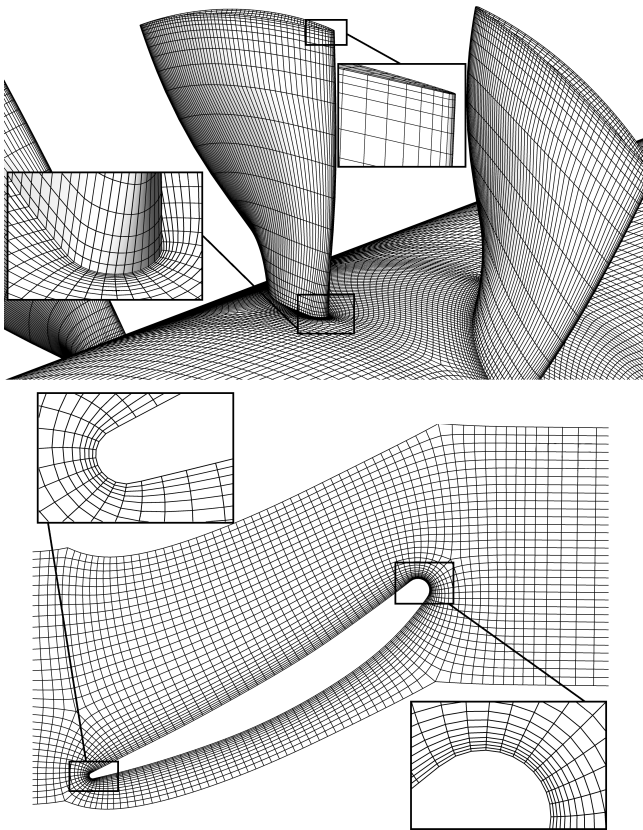


Figure 3. Solid surface mesh structure.

Inlet distortion is enforced by different configurations of screens embedded upstream the rotor blade row. Figure 2 shows geometries of these screens (cases II to VI) together with the non-distorted case (case I). All these distortion screens block the same portion of the main flow of the compressor annulus passage by 25%.

Multi-block structured mesh system has been used for the numerical modelling. Mesh structure distributed on the solid boundaries are shown in Fig. 3. The meshes are clustered towards the solid boundaries in order to meet $y^+ < 5$;

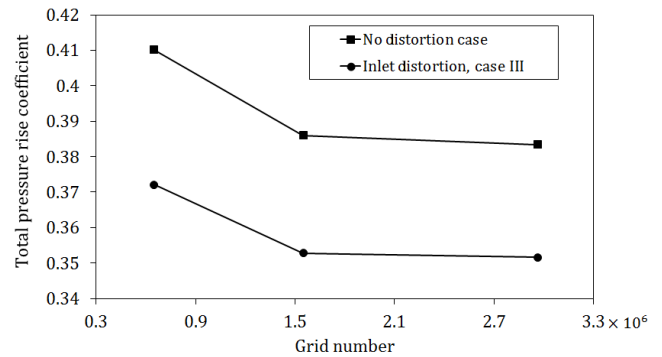


Figure 4. Grid independency results.

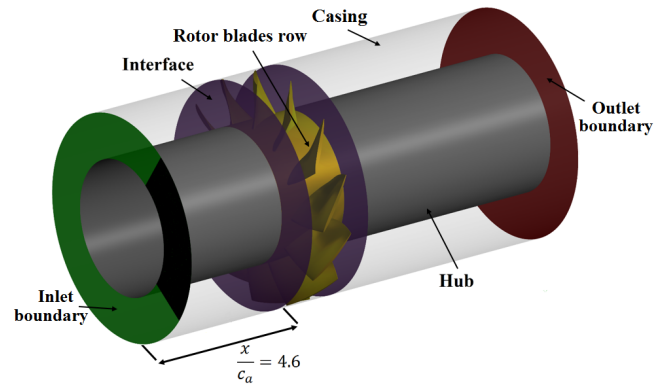


Figure 5. Boundary conditions of solution domain.

necessary condition for a precise simulation of flow within the boundary layer. The total number of meshes was around 1 600 000 for each configuration. Grid independency test has been checked for the clear inlet (i.e., no distortion screen) and one inlet distortion (case III) conditions. The number of grids in the entire solution domain especially within the blade row tip region, was altered and its effect on the total pressure rise coefficient and efficiency was studied. Mesh independency results are shown in Fig. 4 for the whole annulus, which suggest that the suitable numbers of the grids would be about 1 600 000.

Boundary conditions of the solution domain and axial position of the distortion screens are shown in Fig. 5. The boundary conditions are as follows:

- Flow velocity and its direction on the inlet boundary,
- Smooth and adiabatic solid walls, and
- Radial equilibrium assumption on the outlet boundary.

The turbulence model of $k - \omega$ SST has been used through the calculations.

The commercial computational fluid dynamics software of ANSYS-CFX 15.0 was used for the present flow simulations. Its two elements of ANSYS CFX-Pre and CFX-Solver

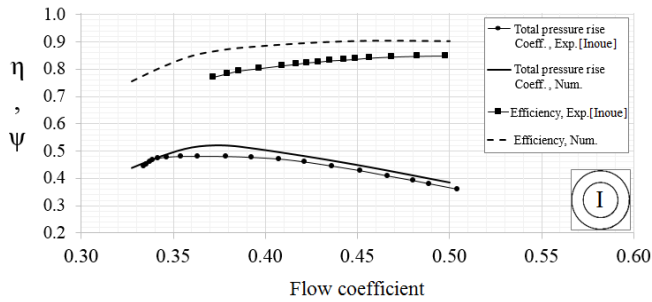


Figure 6. Comparison between present numerical performance maps with experimental results of Inoue and Kuroumaru (1989).

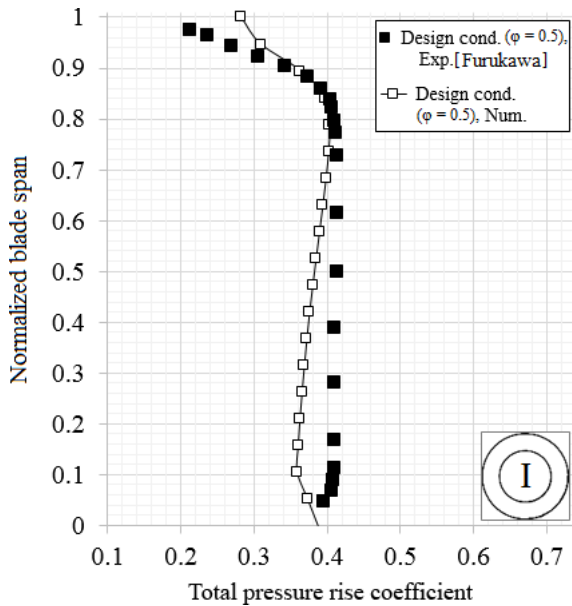


Figure 7. Comparison between present numerical total pressure rise coefficient with experimental results of Furukawa et al. (1998).

were used for defining of boundary conditions and solving the governing equations, respectively. In addition, post processing of the results was executed by CFX-Post software. The computational domain which is shown in Fig. 5, consist of three blocks. The first and the last blocks are stationary and the middle one, which is around the rotor blades row, rotates at a constant speed of 1300 r min^{-1} . The general grid interface (GGI) was used for connection between the stationary and rotating blocks. An implicit second-order Euler method was used for temporal discretization and a second-order high-resolution scheme was employed for spatial discretization of the governing equations. A time step of $3.2 \times 10^{-5} \text{ s}$, which is equivalent to 120 time steps for each blade passing period, has been considered for the numerical purposes.

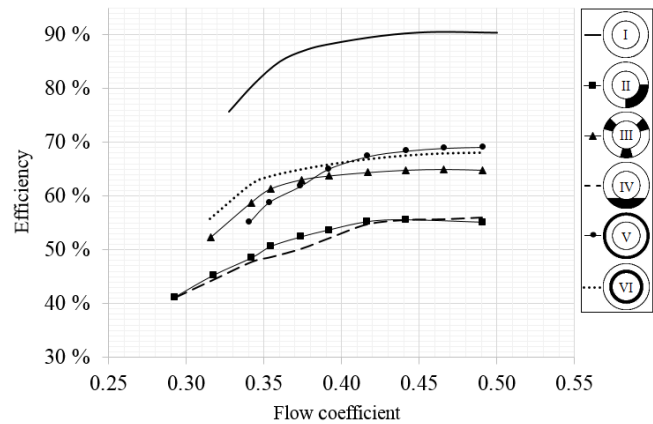
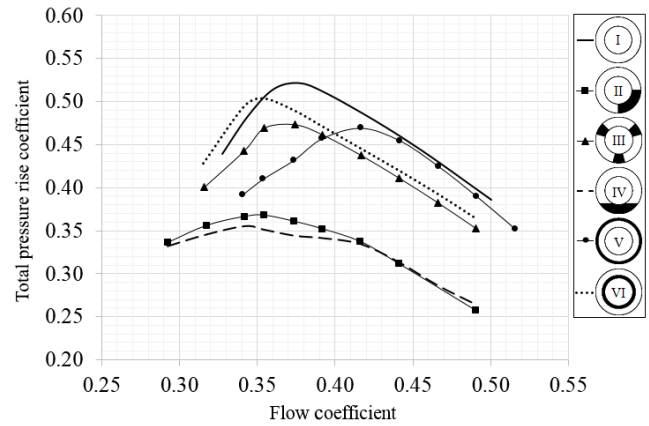


Figure 8. Performance curves for different cases.

3 Validation of present numerical approach

To validate the present numerical approach, performance curves in terms of total pressure rise coefficient (ψ) and efficiency (η) versus flow coefficient (ϕ) for non-distorted case are compared with Inoue and Kuroumaru's (1989) experimental results. These results are shown in Fig. 6. In addition, as shown in Fig. 7, the general trend of the spanwise distribution of the total pressure rise coefficient for undistorted case and at the design point condition ($\phi = 0.5$, $\psi = 0.4$) is compared with experimental results of Furukawa et al. (1998). It can be deduced that the general trend of the current numerical results, presented in Figs. 6 and 7, is nearly in consistent with the relevant available experimental results.

4 Performance curves

Numerical results extracted from the current analyses provided to obtain the compressor performance curves in terms of the total pressure rise coefficient and efficiency versus the flow coefficient. Figure 8 shows these results. Obviously, non-blocked case is accompanied by the best performance, i.e., the highest loadings and efficiencies. The worst cases belong to the non-symmetric blockages, i.e., those due to the par-

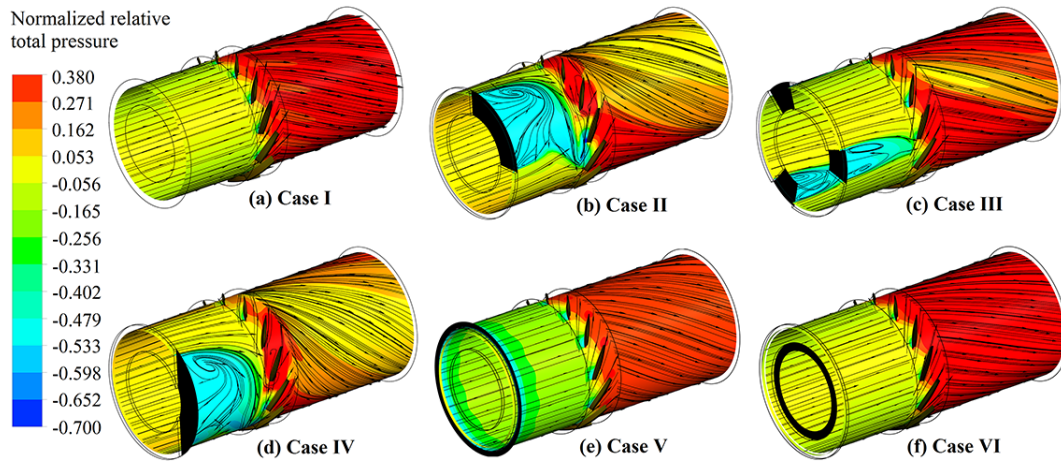


Figure 9. Normalized relative total pressure contours and streamlines on 80 % span circumferential plane at design condition.

tial circumferential blockages (cases II and IV). Inner and outer continuous circumferential distortion screens (cases V and VI) produce better performances in comparison to the other blockage cases. However, the former case exhibit better than the latter one. Outer continuous circumferential distortion screen (case V) worsens the rotor blade tip leakage flow characteristics and consequently causes earlier stall of the blade row tip region (i.e., at a higher flow coefficient) in comparison to the other cases.

It can be concluded that the non-symmetric screens considerably deteriorate the compressor performance at the same blockage ratio. This is due to large wakes produced behind the screens which can increase the losses, significantly. This fact is confirmed in the next section which is devoted to the flow field structure results for all the test cases.

5 Flow fields results

For the sake of brevity, results of only two extreme cases of far stall (i.e., design point) and near stall conditions are considered for presentation and discussions in this section.

5.1 Design point results

Figure 9a to f show flow field results for undistorted and distorted cases which are all operating at the design point condition with $\varphi = 0.5$. These results, presented relative to the rotating frame, are in terms of the normalized relative total pressure (with respect to $0.5\rho u_t^2$) contours and streamlines on a cylindrical surface which cut the blades at their 80 % span. Large wake sizes behind the discrete distortion screens (cases II, III and IV) can be observed in this Figure. The worst cases belong to cases II, IV which are definitely accompanied by deterioration of the rotor blade row performance (see also performance curves in Fig. 8). Their undesirable effects (i.e., non-uniformity in the total pressure) downstream the rotor blade row area can be easily detected

by referring to Fig. 9b to d. Inner and outer continuous circumferential screens (cases V and VI) induce no significant distortions to the entrance flow of the rotor blade row. Consequently, their performance curves would be better than the previous cases (refer to Fig. 8, too).

Flow fields contours for various distortion cases are shown in Fig. 10 at design point condition, relative to a rotational frame fixed to the rotor blade row. Figure 10a shows the normalized relative total pressure contours for all the six cases on a plane located at 50 % of the blade axial chord length measured from its leading edge ($x/C_a = 0.5$). Once again, one can realize that the worst cases belong to cases II and IV. Normalized axial velocity (C_x/u_t) contours are also shown in Fig. 10b for three selected cases of V, VI and non-distorted ones on the same plane of $x/C_a = 0.5$. No considerable blockages can be observed for these cases in comparison to the other distortion screens. Normalized axial velocity contours on a 98 % span circumferential plane are shown in Fig. 10c for non-distorted and II, III and IV cases. Considerable reversed flow zones, designated by blue colour, have happened for cases II and IV which have wrapped around about 5 blades at any instant. These reversal flows cause the axial velocity flow to reduce and consequently the flow incidence to increase, which in turn, could lead to early separation of the flow from the blades leading edges. The intensity of this blockage can be so high to cause the compressor to operate close to the unstable situation.

5.2 Near stall results

The same types of results as those for the design point condition (Sect. 5.1) are presented in this section. Figure 11a to f show normalized relative total pressure contours and surface streamlines for the undistorted and distorted cases at the near stall condition ($\varphi = 0.37$) in the rotating frame. Cases II, III and IV induce again the biggest wake sizes and consequently produce the largest losses. It can be realized that the

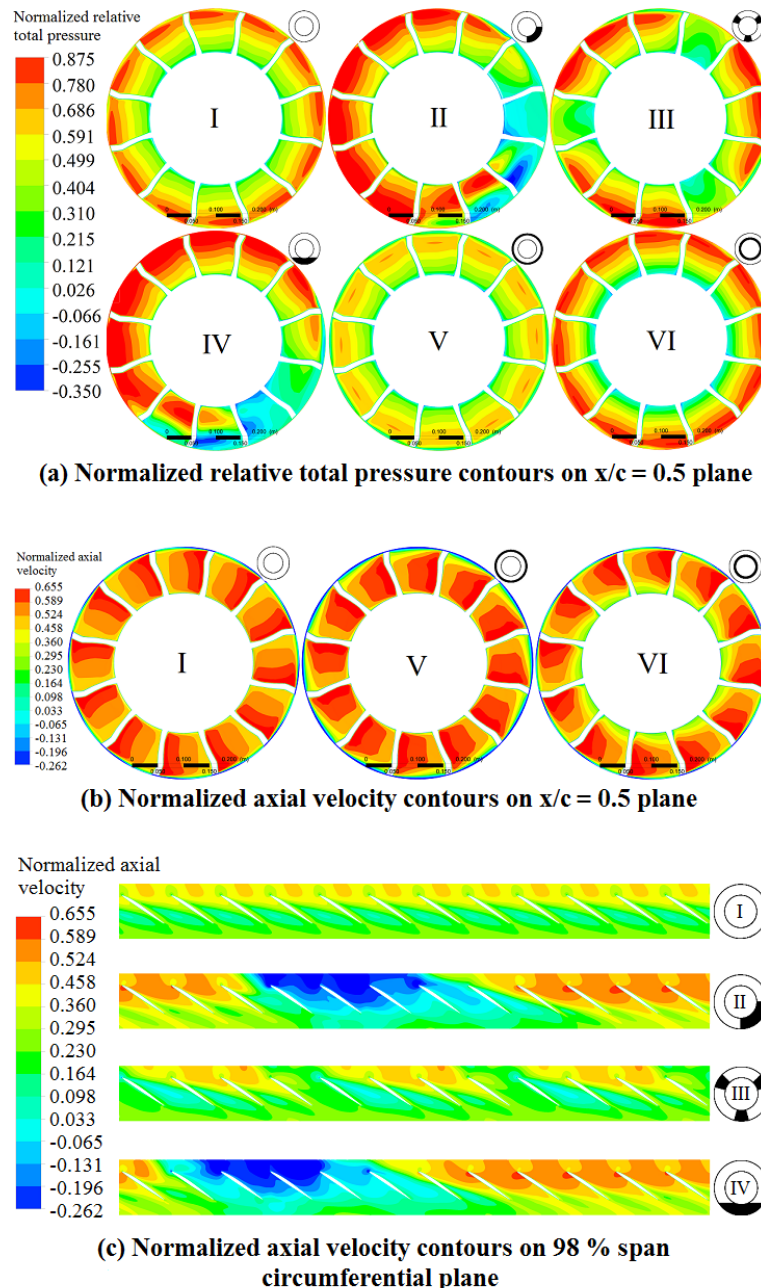


Figure 10. Flow fields for various distortion cases at design point condition.

total pressure rise through the rotor blade row has increased in comparison to the design point for all the distortion cases (Fig. 9a to f). In addition, comparing the surface streamlines in the design condition (Fig. 9a to f) with those in the near stall condition (Fig. 11a to f) one can realize that the exit flow angles are higher in the latter case.

According to the results presented in Fig. 8, the efficiency of case III is more than case V in the design condition. But, it is vice versa at the near stall point. This fact happens in spite of the larger wake size of case III in comparison to case V.

Time averaged total pressure results, presented in Fig. 11, confirms this fact if one follow the values of the pressures in the two above-mentioned cases. The physics behind this can be explained as follows. Generally speaking, the flow structure in the blade row tip clearance region highly contributes into the flow field properties and losses. The outer radial screen can highly affect the flow field in the blade row tip region. This effect becomes more severe while operating at the near stall condition. In another words, its destructive

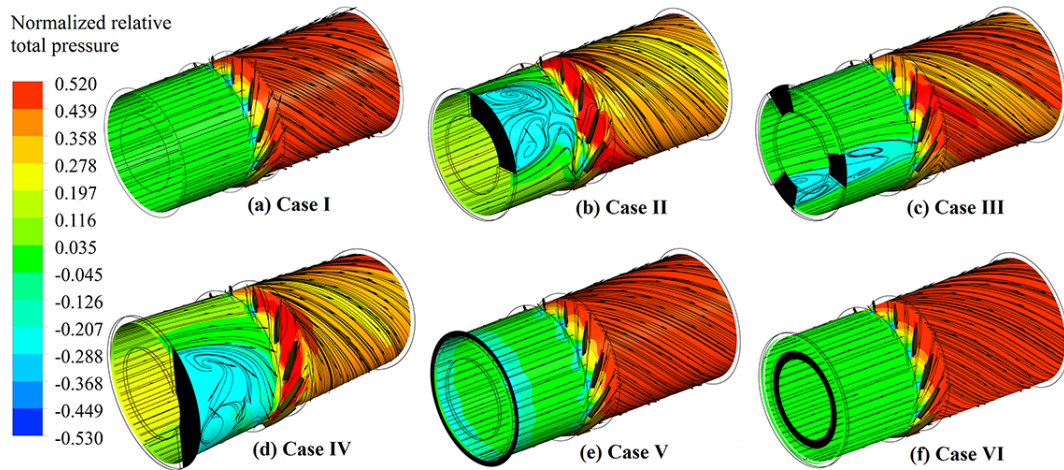


Figure 11. Normalized relative total pressure contours and streamlines on 80 % span circumferential plane at near stall condition.

effects can diffuse through the whole flow passage and cause the efficiency to reduce, considerably.

Referring to Fig. 12a to c, it can be realized that the worst cases belong again to II and IV distortion screens. More intense reversed flow zones, designated by blue colour, have happened for these latter cases with more number of blades engaged with reversal flows in comparison to the design point condition.

6 Spanwise pressure rise results

Spanwise distributions of the total pressure rise coefficient for various cases are shown in Fig. 13a and b for the design point and the near stall conditions, respectively. Obviously, because of reduction in the mass flow rate at the near stall condition in comparison to that at the design point, the total pressure rise coefficient would be greater for the former case. The worst conditions belong to II and IV cases which are associated with the maximum losses. The largest pressure rise occurs for the non-distorted case at the near stall condition (see Fig. 13b). However, there can be seen more pressure rise above the 80 % span for case V and below 30 % span for case VI in comparison to the non-disturbed case. The same trend can be observed for the design point case, but, obviously with lower values (see Fig. 13a). The reason for such a behaviour is explained in the following paragraph.

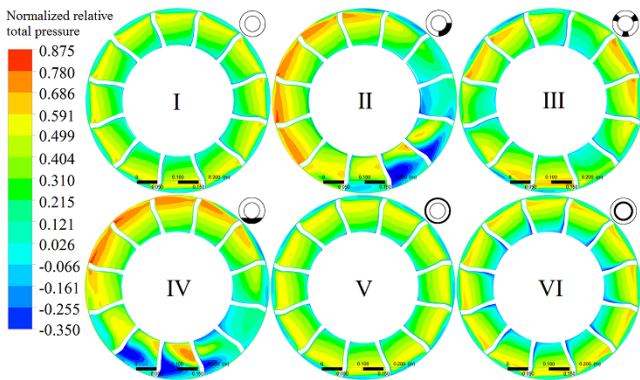
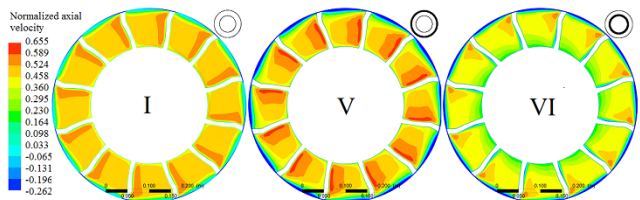
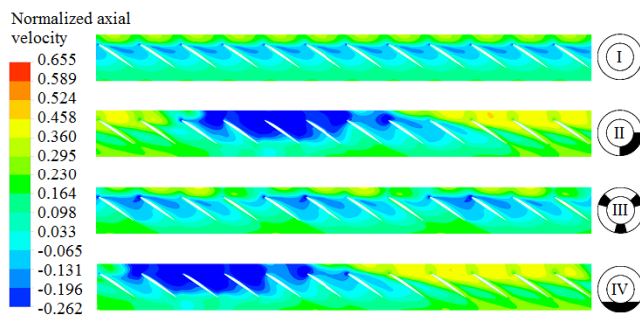
Referring to Fig. 9e and f and Fig. 11e and f it can be detected that V and VI cases have produce the smallest blockages to the main stream. In addition, as has already been mentioned, the best performances belong to these two latter cases among all the distorted ones (see Fig. 8). In fact, these two kinds of screens cause the local mass flow rate behind them to reduce, whilst the local efficiency does not change considerably. Referring to Fig. 13a and b one can realize that this behaviour takes place for cases V and VI above 80 % span and below 30 % span, respectively, where the total pres-

Table 1. Reduction in spanwise averaged total pressure rise coefficient relative to the undistorted case.

Distortion Screen	$\Delta\omega$ (Design Point)	$\Delta\omega$ (Near stall cond.)
	30.5 %	29.2 %
	4.3 %	5.3 %
	28.3 %	32.3 %
	1.9 %	7.7 %
	0.3 %	1.8 %

sure rise coefficient increases. Under these circumstances the blade row experiences higher loading, due to the less drop in the efficiency in comparison to the other cases. As has already been mentioned, other cases are associated with larger wakes and consequently with higher losses.

Table 1 summarizes reduction in spanwise averaged total pressure rise coefficient relative to the undistorted case ($\Delta\omega$) for different distortion screens at design point and near stall condition. It can be observed that the highest losses belong to cases II and IV.

(a) Normalized relative total pressure contours on $x/c = 0.5$ plane(b) Normalized axial velocity contours on $x/c = 0.5$ plane

(c) Normalized axial velocity contours on 98 % span circumferential plane

Figure 12. Flow fields for various distortion cases at near stall condition.

7 Conclusions

Effects of inlet distortions on performance of an axial compressor rotor blade row are studied using computational fluid dynamic technique. Various distortions are imposed by embedding five screens of different geometries, but, with the same blockage ratio. The main conclusions drawn from the current research work can be stated as follows:

The worst cases belong to non-symmetric blockages, i.e., partial circumferential blockages, which are accompanied by largest wakes and consequent considerable losses.

Inner and outer continuous circumferential distortion screens showed better performances in comparison to non-symmetric blockage cases. The outer continuous circumferential screen exhibits better than the inner one for situations

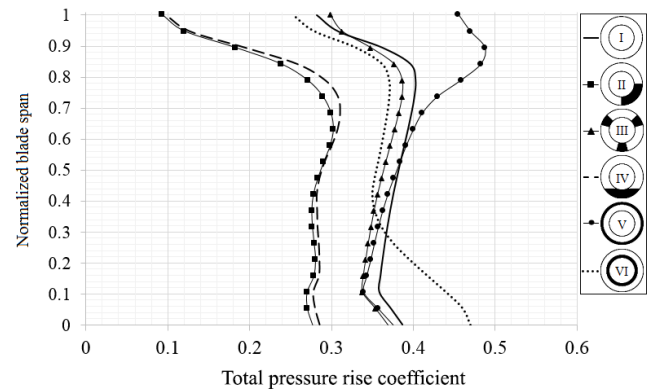
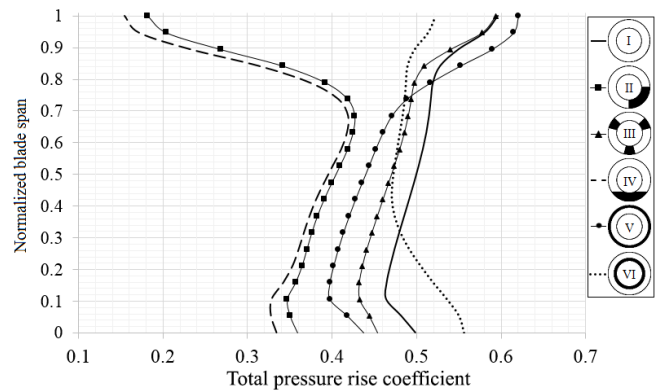
(a) Design point cond. ($\phi = 0.5$)(b) Near stall cond. ($\phi = 0.37$)

Figure 13. Spanwise distributions of total pressure rise coefficient for different cases.

close to the design point. However, it is vice versa at the near stall conditions.

Outer continuous circumferential distortion screen worsens rotor tip leakage flow characteristics and consequently causes early stall of blade tip region.

Data availability. All datasets used in the manuscript can be requested from the corresponding author.

Appendix A

Nomenclature

P_0	Total Pressure
ρ	Air density at the rotor blades row entry
u_t	Blade row tip speed
C_x	Axial velocity at the rotor blades row entry
C_a	Blade axial chord
ψ	Loading coefficient = $\frac{\Delta P_0}{0.5\rho u_t^2}$
φ	Flow coefficient = $\frac{C_x}{u_t}$
η	Efficiency

Competing interests. The authors declare that they have no conflict of interest.

Acknowledgements. Financial support of Aerodynamics and Compressible Turbomachine Research Laboratory of the Iran University of Science and Technology for conducting this research work is highly appreciated.

Edited by: A. Barari

Reviewed by: S. Rane and three anonymous referees

References

- Berrier, B. L. and Allan, B. G.: Experimental and computational evaluation of flush-mounted, S-duct inlets, *AIAA Paper*, 764, 1–15, 2004.
- Charalambous, N., Ghisu, T., Iurisci, G., Pachidis, V., and Pilidis, P.: Axial compressor response to inlet flow distortions by a CFD analysis, *ASME Turbo Expo, Power for Land, Sea, and Air*, 5, 1637–1649, 2004.
- Dong, X., Sun, D., Li, F., Jin, D., Gui, X., and Sun, X.: Effects of Rotating Inlet Distortion on Compressor Stability With Stall Precursor-Suppressed Casing Treatment, *J. Fluid. Eng.*, 137, 111101, doi:10.1115/1.4030492, 2015.
- Furukawa, M., Inoue, M., Saiki, K., and Yamada, K.: The role of tip leakage vortex breakdown in compressor rotor aerodynamics, *ASME 1998 International Gas Turbine and Aeroengine Congress and Exhibition*, 1998.
- Hah, C., Rabe, D. C., Sullivan, T. J., and Wadia, A. R.: Effects of inlet distortion on the flow field in a transonic compressor rotor, *J. Turbomach.*, 120, 233–246, doi:10.1115/1.2841398, 1998.
- Inoue, M. and Kuroumaru, M.: Structure of tip clearance flow in an isolated axial compressor rotor, *J. Turbomach.*, 111, 250–256, doi:10.1115/1.3262263, 1989.
- Jian, H. and Hu, W.: Numerical investigation of inlet distortion on an axial flow compressor rotor with circumferential groove casing treatment, *Chinese J. Aeronaut.*, 21, 496–505, 2008.
- Lee, K.-J., Lee, B.-H., Kang, S.-H., Jung, J.-H., Yang, S.-S., Lee, D.-S., and Kwak, J.-S.: Development of Block type Inlet Distortion Simulating Device for Gas Turbine Engine Inlet Distortion Test, *International Journal of Aeronautical and Space Sciences*, 8, 121–125, doi:10.5139/IJASS.2007.8.2.121, 2007.
- Lee, K., Lee, B., Kang, S., Yang, S., and Lee, D.: Inlet Distortion Test with Gas Turbine Engine in the Altitude Engine Test Facility, *AIAA Paper*, 4337, doi:10.2514/6.2010-4337, 2010.
- Liu, K., Sun, Y., Zhong, Y., Zhang, H., Zhang, K., and Yang, H.: Numerical investigation on engine inlet distortion under crosswind for a commercial transport aircraft, 29th Congress of the International Council of the Aeronautical Sciences, St.Petersburg, Russia, 2014.
- Lucas, J. R., O'Brien, W. F., and Ferrar, A. M.: Effect of BLI-Type Inlet Distortion on Turbofan Engine Performance, *ASME Turbo Expo 2014: Turbine Technical Conference and Exposition*, 2014.
- Raj, A. S. and Pandian, P. P.: Numerical simulation of static inflow distortion on an axial flow fan, *International Journal of Mechanical Engineering and Robotics Research*, 3, 20–25, 2014.
- Zhipeng, L., Chao, L., Hui, W., Xiaopeng, L., and Guowang, Z.: Applying CFD Technology to Determine the Effect of Two New Designed Fan Inlet Distortion Generators, *Procedia Engineering*, 99, 646–653, doi:10.1016/j.proeng.2014.12.584, 2015.